Improvements on the FANTASIO set-up and new spectroscopic results concerning the Ar-H_2O van der Waals complex in the 2OH overtone region

A. S. Bogomolov[1,2], R. Glorieux[1*], M. Herman[3], T. Corbo[1], S. Collignon[1], B. M. Hays[1,4], D. Lederer[5], N. Moazzen-Ahmadi[6], A. Libert[1], B. Tomasetti[1], J. Fréreux[1], C. Lauzin[1]*

[1] *Institute of Condensed Matter and Nanosciences, Université catholique de Louvain, Louvain-la-Neuve, Belgium*

[2] *Voevodsky Institute of Chemical Kinetics and Combustion, Novosibirsk, Russia*

[3] *Spectroscopy, Quantum Chemistry and Atmospheric Remote Sensing, Faculté des Sciences, Université Libre de Bruxelles, Brussels, Belgium*

[4] *Physique des Lasers Atomes et Molécules, CNRS, Université de Lille, Lille, France*

[5] *Institute of Information and Communication Technologies, Electronics and Applied Mathematics, Université catholique de Louvain, Louvain-la-Neuve, Belgium*

[6] *Department of Physics and Astronomy, University of Calgary, Calgary, Canada*

** Both authors contributed equally to this work and should both be considered as first author.*

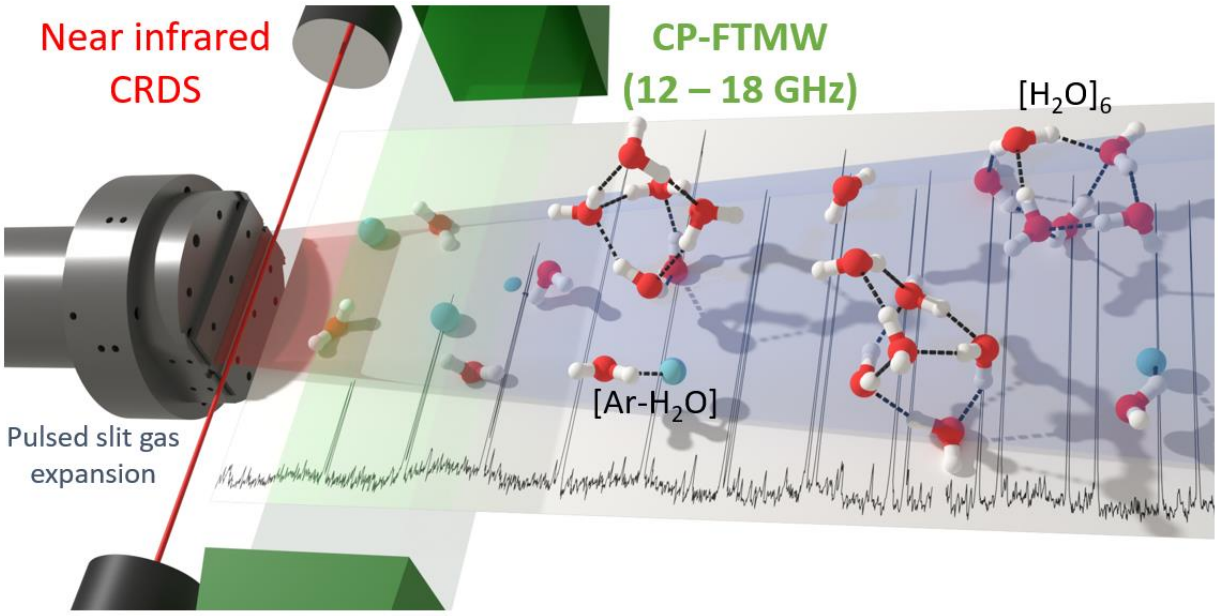

Keywords

Cavity ring-down spectroscopy, slit supersonic jet, water clusters, water-argon, high-resolution spectroscopy

Abstract

We present a series of improvements of the FANTASIO experimental set-up that couples a supersonic expansion to a cavity ring-down spectrometer originally reported by *M. Herman, et al., Mol. Phys.* ***105****, 815 (2007)*. In particular, the implementation of a new pulsed slit valve of 80 mm in length is detailed. The design is based on a powerful piezo stack actuator. Schlieren imaging is used to verify the homogeneity of the molecular beam and the quality of the pulsed slit performance. The ability to form weakly bound van der Waals complexes is assessed using the cavity ring-down spectrometer and a new chirped-pulse Fourier transform microwave spectrometer with the 12-18 GHz operating range. The water hexamer and heptamer were observed using this microwave spectrometer. Following enhancements and an extended laser

coverage of the CRDS in the 2OH region, we observed and analyzed seven sub-bands of the Ar-$H_2{}^{16}O$ van der Waals complex, along with one sub-band of the much less abundant Ar-$H_2{}^{18}O$ isotopologue.

I. Introduction

The high-resolution spectroscopic investigation of van der Waals complexes provides quantitative information on the intermolecular interactions and the dynamics taking place between the molecular entities. Such complexes are usually produced in a supersonic expansion by taking advantage of the non-equilibrium nature of the jet to study the initial steps in the nucleation process. In optical spectroscopy, the use of a slit injector is particularly convenient to increase the interaction length between the light source and the molecular beam. Since the first successful report of a pulsed planar supersonic jet developed for high-resolution spectroscopic studies [1], a series of designs have been presented [2–4]. These designs differ by the choice of the actuator used to provide a vacuum tight slit. More recently, the use of a long piezo stack was implemented to produce a pulsed circular free jet using a Laval nozzle [5]. This work was followed by a report on the production of a pulsed slit [6] using a similar piezo device, requiring a mechanically demanding scheme. In the present work, we describe the design and the experimental characterization of a new pulsed slit valve implemented in the FANTASIO experimental set-up. Our design is directly inspired by the work presented in Ref. [5]. In addition, the first results from a new home-built segmented [7] chirped-pulse Fourier transform microwave (CP-FTMW) spectrometer (in the range of 12-18 GHz) will be presented.

FANTASIO [8–10] is an experimental set-up that was initially built to study van der Waals complexes formed in a continuous supersonic expansion. The species in the beam were probed with a continuous-wave cavity ring-down spectrometer (CRDS with S standing for either spectrometer or spectroscopy) working in the near infrared range (~1.4 microns). Complexes containing acetylene, water or ammonia were investigated in their 2CH, 2OH, and 2NH overtone excitation regions, respectively, as reviewed in Ref. [10]. In the present report, following improvements made on FANTASIO coupled with a broader frequency range, new results on the Ar-H_2O van der Waals complex are presented in the 2OH region. We used the most recent (2017) results obtained on the FANTASIO set-up for Ar-H_2O by Vanfleteren *et al*. [11] to benchmark the improvements achieved on FANTASIO. Vanfleteren *et al.* [11,12] studied the (200) ← (000) and (101) ← (000) vibrational bands of Ar-H_2O, where ($v_1v_2v_3$) indicates the vibrational quantum numbers of the H_2O entity. FANTASIO was also used by Didriche *et al.* [13] to study the (111) ← (000) and (101) ← (000) vibrational transitions of Ar-D_2O and Ar-DOH, respectively. Prior to these reports, the Ar-water complex was first investigated in 1988 by Saykally's group, who studied Ar-H_2O in the far infrared [14–16]. Since then, there have been numerous works on the Ar-water complex in other spectral regions such as the microwave (MW) [17], millimeter wave [18], and mid-infrared [19].

The Ar-water spectrum is usually modeled using pseudo-diatomic expression for the rotation as detailed in Ref. [11]. In this work, the Ar-H_2O complex sub-states will be labeled using the $|M_j|(j_{kakc})$ notation, where j_{kakc} is the rotational level of water to which the sub-state of Ar-water is correlated and M_j the projection of the rotational angular momentum of the water molecule (j) on the intermolecular axis of the complex. The $|M_j| = 0, 1, 2, \ldots$ values are labeled as Σ, Π, Δ, …, respectively. In each sub-state, the overall rotation of the complex is labeled using the total angular momentum quantum number J (with $J \geq |M_j|$). The intramolecular vibrational states will be indicated using the ($v_1v_2v_3$) vibrational quantum numbers of the water monomer entity. All the bands observed in the present work start from the ground intramolecular vibrational state of H_2O.

This paper is organized as follows: a general description of the FANTASIO set-up is provided in Sec. II; the newly implemented pulsed slit, the homogeneity of the molecular beam, the improvements in terms of signal-to-noise ratio (SNR) and cluster production are presented in Sec. III; original results obtained with this new pulsed slit concerning the Ar-H_2O van der Waals complex are presented in Sec. IV, before the concluding remarks in Sec. V.

II. Description of the FANTASIO set-up

FANTASIO stands for "Fourier trANsform, Tunable diode and quadrupole mAss spectrometers interfaced to a Supersonic expansIOn" the set-up was initially presented in Ref. [8]. The set-up was built in Brussels

and moved to Louvain-la-Neuve in 2019. It has been significantly updated since the reports by Didriche *et al*. [9] and Bogomolov *et al*. [20]. The current version of the set-up is presented in Fig. 1. The improvements are highlighted in orange.

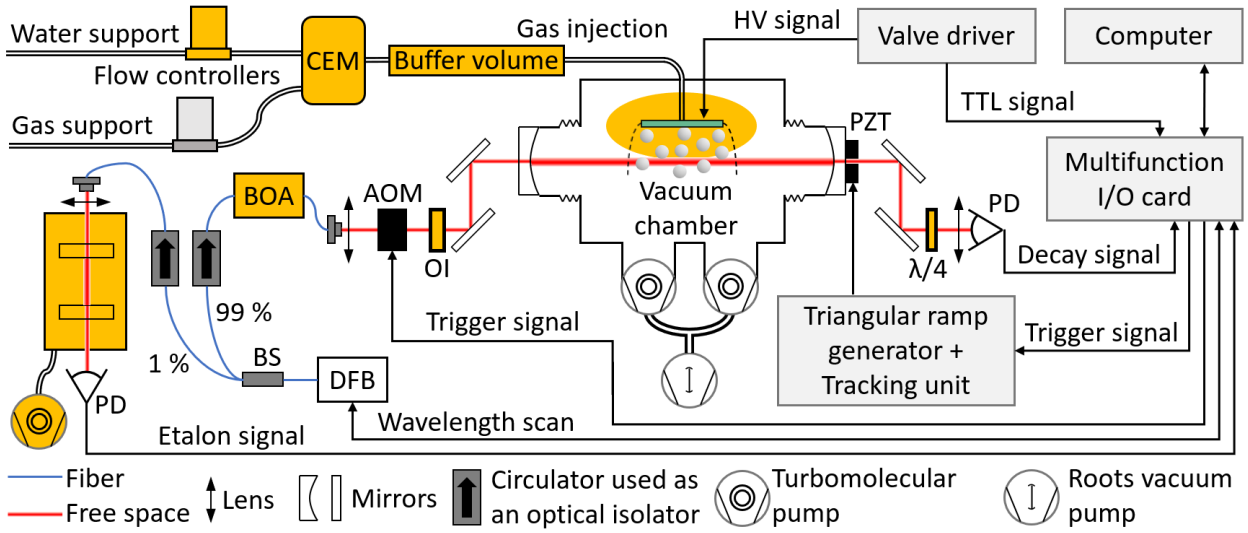

Figure 1. General scheme of the FANTASIO set-up. The improvements in relation to Ref. [20] *are indicated in orange. See text for more details. DFB stands for distributed feedback laser, BS for beam splitter, BOA for booster optical amplifier, AOM for acousto-optic modulator, OI for optical isolator, PZT for piezoelectric transducer, PD for photodiode, and CEM for controlled evaporation mixer. The CRDS and MW are probing the expansion ~1 and 10-70 mm downstream from the slit nozzle respectively. The MW system is not shown for clarity.*

Gas injection and evacuation

The vacuum chamber is pumped by two Leybold MAG W3200 CT turbomolecular pumps backed by an Alcatel ADS 8699 HII primary pump. The pumping capacity of 6400 L/s sets the limit of gas that can be injected into the chamber. The gas mixture for the expansion is prepared using a controlled evaporation mixer (CEM) from Bronkhorst based on F-201 (full scale of 3 standard L/min gas) and M12 (full scale of 30 ml/h liquid) flow controllers. Typical flows are 3 standard L/min of Ar and 1.2 mL/h of liquid water. Between the CEM and the gas valve a 2 L buffer volume is required to improve the pressure and concentration homogeneity.

Cavity ring-down spectrometer

CRDS is used to probe the species formed in the jet. A set of DFB lasers is used as narrow-band light source. This radiation is divided in two parts. On each branch, circulators (CIR) are used as isolators. The main part of radiation is amplified using a booster optical amplifier (BOA1410S from Thorlabs), increasing the power by about a factor 10. Then the radiation is passed through the acousto-optic modulator (AOM, MFAS80-A1 from AA Opto-Electronics) and the deflected branch (120 mW) is aligned with an optical cavity formed by two mirrors (154209 from Layertec) spaced by approximately 75 cm. The optical isolator (OI, IO-4-1390-VLP/M from Thorlabs) and λ/4 waveplate (AQWP05M-1600 from Thorlabs) are used to prevent optical feedback and to damp the presence of parasite etalons. The output mirror of the cavity is mounted on a piezo assembly (PZT) for the cavity length scanning/tuning. The displacement of the mirror is larger than several wavelengths (few microns) to ensure resonance at any laser frequency. At this point, light leaking out of the cavity is detected by the photodiode. At a certain threshold intensity, the AOM is switched off and it thus stops the injection of light into the optical cavity. The light intensity decay is recorded, and the typical time is determined from fitting the signal to an exponential decay curve. The typical decay time is near 135 μs for an empty cavity.

Wavelength calibration

A small portion of the DFB laser radiation is sent into a thermostabilized 75 mm long Fabry Perot resonator with a spacer made of ULE 7972 glass produced by Docter Optics. This resonator is composed of two 90:10 beam splitters (BSX06 from Thorlabs) and is placed under vacuum to minimize pressure and temperature fluctuations. This resonator provides an equidistant comb in frequency that allows to linearize the output signal. Absolute calibration of the linearized spectrum is made using water monomer absorption lines recorded in the jet chamber, along with their frequencies from the HITRAN database [21]. The calibration accuracy is typically 10^{-3} cm^{-1}.

III. The new pulsed slit valve

A new pulsed slit valve was recently incorporated in the FANTASIO setup (see Fig. 2). The main feature of the valve is the very long closing cross section along the length of the slit. The sealing is made by the O-ring mounted around the slit. A 90 mm long plunger made of hardened steel RWL34 is used for closing the nozzle. The use of hardened steel is essential to avoid any distortion of the plunger after a few days of use. The plunger is actuated by a P-212.80 piezo assembly, manufactured by Physik Instrumente. An active-low control signal is sent to the piezo assembly to provide either 800 V to close the valve (1000 V maximum for the assembly) or 0 V for its opening. Under these conditions, the displacement of the plunger is approximately 100 µm. A differential micro screw tunes the position of the piezo stack for optimal functioning along the same line as in Ref. [5]. The optimal screw setting is adjusted to avoid any leaking through the valve while the piezo is energized (800 V). For optimal sealing, the working surface of the plunger must be flat, polished and normal to the displacement direction.

We used Schlieren imaging and absorption of the Ar-H_2O van der Waals complex recorded in the near infrared region to optimize the geometry and the spacing of the blades. A series of nozzle blades profiles were built and tested. The design detailed in Fig. 2e was found to provide the best results, i.e. the best flow direction and homogeneity, along with Ar-H_2O formation. The blades are 50 µm spaced and glued on the sides (Fig. 2b).

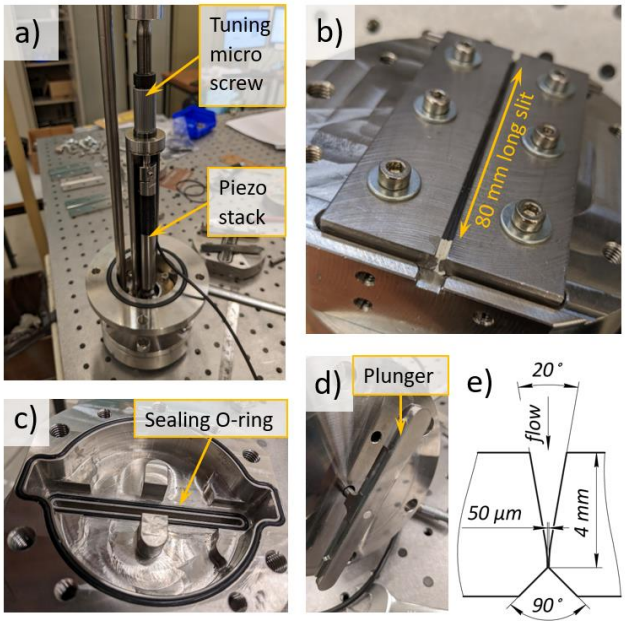

Figure 2. Illustration of the valve design: a) the piezo stack, b) the slit nozzle jaws c) the O-ring mounted around the slit, d) the hardened steel plunger, and e) the jaws profile.

Validation of the new pulsed slit valve: Schlieren imaging to test the molecular beam homogeneity and the mechanics of the new valve

The propagation of CO_2 flowing from a reservoir at pressure of 5 bar to ambient air was imaged using the Schlieren effect [22]. The optical scheme used for these measurements is shown in Fig. 3a. The resulting images made of the difference between images with and without CO_2 flowing out of the valve are shown in Figs. 3b and 3c. The red and blue colors indicate deflection of the light due to gas flowing out of the nozzle. In these figures, the homogeneity along the slit and straightness of the flow can be appreciated. A divergence angle of approximately 30° (Fig. 3c) was determined for this pressure ratio. Several blade designs were tested using this set-up and the vertical alignment of the blades appeared to be critical to avoid any lateral distortion of the expansion, i.e. due to the Coanda effect. In fluid mechanics, this effect is defined as the action whereby a flow along a solid surface tends to follow the curvature of the surface [23].

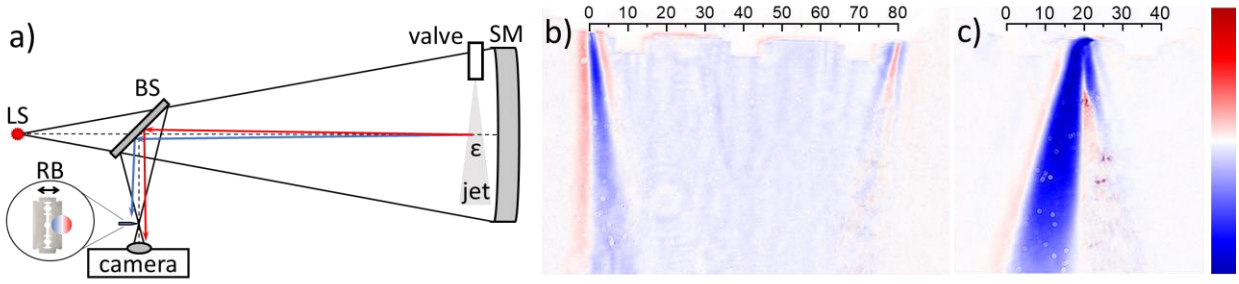

Figure 3. a) The scheme of the Schlieren imaging set-up used to test the new pulsed slit valve and blades alignment. The point source of light (LS) is located at the 2F distance from the spherical mirror (SM). Spatial filtering of the light is produced at the image of the point source using a razor blade (RB). The expansion from the new valve and the variation in density are imaged using a camera. b) is the Schlieren images of the gas along the length of the slit and c) perpendicular to the axis of the slit. Red and blue indicate a maximum and a minimum light intensity, respectively. The scale on top indicates the size of the expansion in mm.

Validation of the new pulsed slit valve: Assessing the formation of van der Waals complexes.

Once the mechanics of the new valve was validated, it was installed on the FANTASIO set-up to replace the pulsed valve based on a Parker 9 valve coupled to a multichannel block [20]. The new pulsed slit valve is typically operated at 4 Hz with a pulse duration of 20 ms. Ring-downs are recorded during 15 ms after a 5 ms delay while the jet is ON, and for 180 ms after a 50 ms delay while the jet is OFF. The absorption in the cavity recorded without injection is subtracted from absorption during the pulse, as detailed in Ref. [20]. This measurement scheme allows us to record the spectrum independently of some experimental parameters variation such as the mirror reflectivity and the absorption of the residual background gas in the chamber. A comparison of SNR for the same acquisition time for a small portion of the Ar-H_2O spectrum around 7208 cm^{-1} is shown in Fig. 4. An improvement in SNR is clearly observed. This increase in SNR arises from the cumulative effect of the signal increase thanks to the new pulsed slit valve and the better sensitivity of the set-up, obtained by isolating the cavity from the main frame, amplifying light using BOA, and the better gas injection using CEM. The observed rotational temperature of spectra taken a few mm away from the new valve exit is estimated to be 13 K. An exciting outcome was the observation of the Ar-$H_2{}^{18}O$ complex in natural abundance (as discussed further in Sec. IV), further confirming the improvement in SNR.

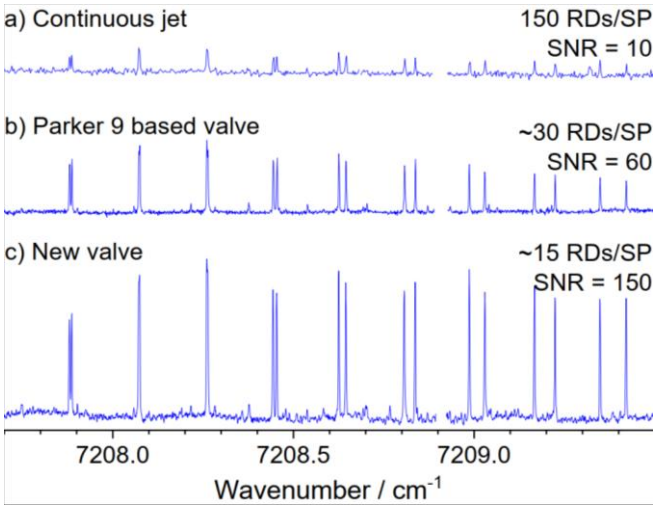

Figure 4. The SNR improvements illustrated by the absorption spectrum of Ar-H_2O in the region of the $\Pi(1_{10}),(200) \leftarrow \Pi(1_{01}),(000)$ sub-band recorded using CRDS. The number of ring-downs per spectral point (RDs/SP) measured while the expansion is active for around 1.5 second acquisition time are indicated. Plenty of small lines appear from the noise background in panel c), so from the first view, it can be seen as an increase in the noise, but this is not the case. Therefore the ~~The~~ SNRs are calculated for the strongest line at 7208.26 cm^{-1} right next to the line. The top trace was reported by Vanfleteren et al. [11].

The same gas expansion was probed downstream using a CP-FTMW spectrometer, based on that reported in Ref. [24], to observe large clusters and assess the cooling capabilities of the expansion. The details of this new spectrometer will be provided in a subsequent publication. Briefly, MW pulses of ~1 µs are swept over a 500 MHz bandwidth within the 12-18 GHz frequency range, amplified to a 10 W power level and broadcasted through the molecular beam by a horn antenna. After excitation, the free induction decay (FID) signal emitted by the polarized gas is collected by a second horn antenna, amplified with a 48 dB gain, and down converted in frequency to be digitized by a 1 GSa/s oscilloscope. The spectrum is then obtained by Fourier transformation of the acquired FID, over a typical 15 us time window. Thanks to the phase stability enforced throughout the spectrometer by a GPS-disciplined quartz oscillator, molecular signals can be averaged more than a 1 million times to improve the SNR. The blue, truncated spectrum shown in Fig. 5 results from the average of 240,000 FIDs, measured in an expansion of H_2O seeded in Ar. For this experiment, the pulsed valve was operated at 5 Hz with a pulse duration of 8 ms. For each gas pulse, a train of 100 FIDs was captured over a 2 ms duration. A time delay of 1.2 ms was set between this acquisition sequence and the rising edge of the TTL signal that drives the pulsed valve. In this configuration, the effective data acquisition is 500 Hz. It thus took 96 minutes of overall measurement time to cover the 12 spectral segments of the full instrumental bandwidth. The Ar and H_2O flows entering the CEM were set to 1.5 L/min and 1.9 mL/h, respectively. The resulting gas mixture was held at a stagnation pressure of 0.8 bar and pulsed in the vacuum chamber at a residual pressure of 10^{-3} mbar. In this spectrum, pure rotational transitions of water hexamer and heptamer can be observed [25,26]. Figure 5 thus illustrates the ability of the new valve to form large aggregates. The observed relative intensity matches with a rotational temperature at the Kelvin level. This estimate was obtained from the adjustment of the calculated relative line intensities to best reproduce the experimental CP-FTMW spectrum of the water hexamer. The stark difference between the rotational temperature of the complexes probed with MW and near infrared light can be rationalized considering the fact that the two spectrometers are working at different positions from the nozzle. In the case of the CRDS, the laser probes the molecular beam a few millimeters from the nozzle whereas in the MW case, the horns are placed more than ten centimeters downstream, hence probing the much cooler region of the expansion. Note that in the MW experiment, the decrease of density is nicely counterbalanced by a significantly larger volume of interaction.

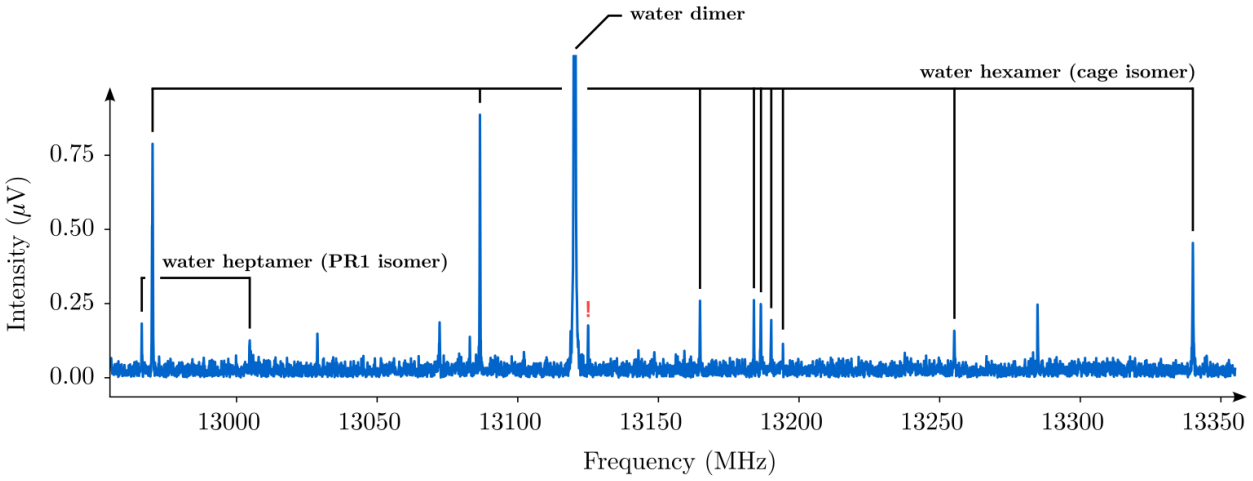

Figure 5. CP-FTMW spectrum of an expansion of H_2O seeded in Ar (see main text for experimental details). Spectral lines associated to water clusters are assigned based on the works in Refs. [25,26]. *The line marked by the red exclamation indicates a spurious tone introduced by the spectrometer electronics. The remaining spectral features are as yet unassigned.*

IV. New spectroscopic results concerning the Ar-water van der Waals complex

Assignment of an Ar-$H_2{}^{18}O$ sub-band

In the spectral region used for benchmarking the improvements of FANTASIO, shown in Fig. 4, a series of regularly spaced weak lines are observed using the Parker 9 valve. This previously unreported sub-band is again observed with the new valve and is assigned to the $\Sigma^e(0_{00}),(101) \leftarrow \Sigma^e(1_{01}),(000)$ ortho sub-band of the Ar-$H_2{}^{18}O$ complex. The assignment is based on lower state combination differences using MW transitions from Ref. [17]. Further support for the assignment of this sub-band are the comparable vibrational shift with respect to the $0_{00},(101) \leftarrow 1_{01},(000)$ transition of the water monomer (4.627 cm^{-1} for Ar-$H_2{}^{18}O$ compared to 4.001 cm^{-1} for Ar-$H_2{}^{16}O$ [11,21]) and the strongest band of Ar-$H_2{}^{16}O$ in this region.

A close up of the experimental spectrum (blue trace) along with the simulated spectrum (red trace) based on parameters listed in Table 1 is shown in Fig. 6a. This simulation was performed using the Pgopher software [27], which was also used for the simulations shown hereafter. This sub-band is labeled as ζ in Table 2. The *P*(6) transition marked with an asterisk is perturbed. It has an obs.-calc. value of about two times the root-mean-square deviation of the fit. In this figure, the strong experimental (blue) and simulated (black) transitions belong to the $\Pi(1_{10}),(200) \leftarrow \Pi(1_{01}),(000)$ sub-band (labeled A in Ref. [11]). The assignment of η sub-band is discussed in the next section.

The $\Sigma^e(0_{00}),(101) \leftarrow \Sigma^e(1_{01}),(000)$ sub-band of Ar-$H_2{}^{18}O$ was analyzed by constraining the $\Sigma^e(1_{01}),(000)$ ground state constants at values from Ref. [17]. The $H_2{}^{18}O$ isotopologue of water was present in natural abundance in the gas mixture. This represents 0.2 % of the $H_2{}^{16}O$ concentration [21]. The observation of this first OH overtone band of Ar-$H_2{}^{18}O$ in natural abundance, with a SNR of about 5, is a strong demonstration of the high sensitivity achieved with the FANTASIO spectrometer in its current state.

Table 1. Molecular parameters for ortho Ar-$H_2{}^{18}O$ (in cm^{-1}).

Sub-state	*e*/*f*	ν_0	*B*	$D(\times 10^6)$
$\Sigma(1_{01})$, (000) [a]	*e*	0	0.090770895	1.901315
$\Sigma(0_{00})$, (101) [b]	*e*	7209.75031(28)	0.0921902(47)	3.327(15)

[a] Fixed ground state constants from Ref. [17].
[b] Quantities in parentheses are 1σ from the least-squares fit, in units of the last quoted digits.

Observation of new Ar-$H_2{}^{16}O$ sub-bands

Taking advantage of the increased sensitivity of the new set up and an increased laser coverage provided by a new DFB laser head with 30 cm^{-1} tunability, a series of new sub-bands for Ar-$H_2{}^{16}O$ were observed between 7165 and 7235 cm^{-1}. These are listed in Table 2 and are labeled using lowercase Greek letters. The experimental intensity of each sub-band is given relatively to the strongest sub-band observed in this region which is $\Sigma^e(0_{00}),(101) \leftarrow \Sigma^e(1_{01}),(000)$, which was given an intensity of 100 in the present measurements. Ortho and para nuclear spin isomers are discussed separately in what follows.

Table 2: Observed and calculated band centers of Ar-H_2O (in cm^{-1}).[a]

#	Obs.	Calc. [b]	Assignment	*o*/*p* [c]	Remarks	Rel. int. [d]
α	7169.330	7170.993	$\Sigma^e(0_{00}),(200) \leftarrow 1\Sigma^e(0_{00}),(000)$	*p*	/	0.5
β	7174.181	7176.416	$\Pi(1_{01}),(200) \leftarrow \Sigma^f(1_{10}),(000)$	*o*	/	0.8
γ	7177.720	7180.437	$\Sigma^e(1_{01}),(200) \leftarrow \Pi(1_{10}),(000)$	*o*	/	4
δ	7187.643	/	/	/	*Q*-branch only	0.4
ε	7189.165	7191.128	$\Pi(1_{01}),(200) \leftarrow \Pi(1_{10}),(000)$	*o*	/	2
ζ	7209.750	/	$\Sigma^e(0_{00}),(101) \leftarrow \Sigma^e(1_{01}),(000)$	*o*	Ar-$H_2{}^{18}O$	0.3
η	7210.327	7212.025	$\Pi(1_{01}),(200) \leftarrow \Sigma^e(1_{01}),(000)$	*o*	/	0.9
θ	7223.490	/	/	/	Perturbed [g]	6

[a] Sub-bands are listed with increasing wavenumber and are labeled using lowercase Greek letters. All sub-bands originate from the monomer (000) ground vibrational state.
[b] From the work of Vanfleteren *et al*. [11].
[c] Ortho (*o*) or para (*p*) state.
[d] Relative intensities with respect to the strongest sub-band in this region $\Sigma^e(0_{00}),(101) \leftarrow \Sigma^e(1_{01}),(000)$, with intensity set to 100 from present measurements.
[g] Strong and perturbed *Q*-branch observed with possible *P* and *R* transitions (see text).

Assignment of the para sub-band

The only sub-band assigned to the para species is the α sub-band. Although very weak, it displays *P* and *R* progressions but no *Q*-branch, hallmark of a $\Sigma \leftarrow \Sigma$ transition. The lower state combination differences indicate that the initial state of this band is the intermolecular van der Waals stretch excitation of the para state denoted by $1\Sigma(0_{00}),(000)$. This state was reported in Ref. [15] with a band origin at 30.265 cm^{-1}. It was found to be strongly mixed with the close lying $\Sigma(1_{11}),(000)$ state, as well as the $\Pi(1_{11}),(000)$ and possibly another unassigned Σ sub-state [16]. This is the likely explanation for the observation of an otherwise forbidden $\Delta k_a = \Delta k_c = 0$, $\Sigma(0_{00}),(200) \leftarrow 1\Sigma(0_{00}),(000)$ transitions. The only possible assignment for the upper state of the α sub-band is the para $\Sigma(0_{00})$ sub-state in (200), predicted to be at 7201.705 cm^{-1} [11]. Due to inconsistencies observed during the rotational analysis of the α sub-band, a new rotational analysis of millimeter wave data in Ref. [15] was carried out with the resulting parameters reported in Table 3. The lower state parameters were kept fixed to obtain the parameters for $\Sigma(0_{00}),(200)$. The results are reported in Table 3.

Table 3. Molecular parameters for para Ar-H_2O of the α sub-band (in cm^{-1}) [a].

Sub-state	*e*/*f*	ν_0	*B*	$B_{Calc.}$ [b]	$D(\times 10^6)$	$H(\times 10^9)$
$\Sigma(0_{00}),(000)$ [c]	*e*	0	0.099678437	0.0993	3.2039	−0.237
$1\Sigma(0_{00}),(000)$ [d]	*e*	30.2650217	0.09467836	0.0957	2.1194	−3.462
$\Sigma(0_{00}),(200)$	*e*	7199.59493(32)	0.0992586(82)	0.0992	3.459(39)	

[a] Quantities in parentheses are 1σ from the least-squares fit, in units of the last quoted digits.
[b] Value of *B* calculated in Ref. [11].
[c] From Ref. [11].
[d] Fixed ground state constants from Ref. [15] retrieved by refitting the $1\Sigma(0_{00}),(000) \leftarrow \Sigma(0_{00}),(000)$ millimeter wave transitions in Table I of this reference.

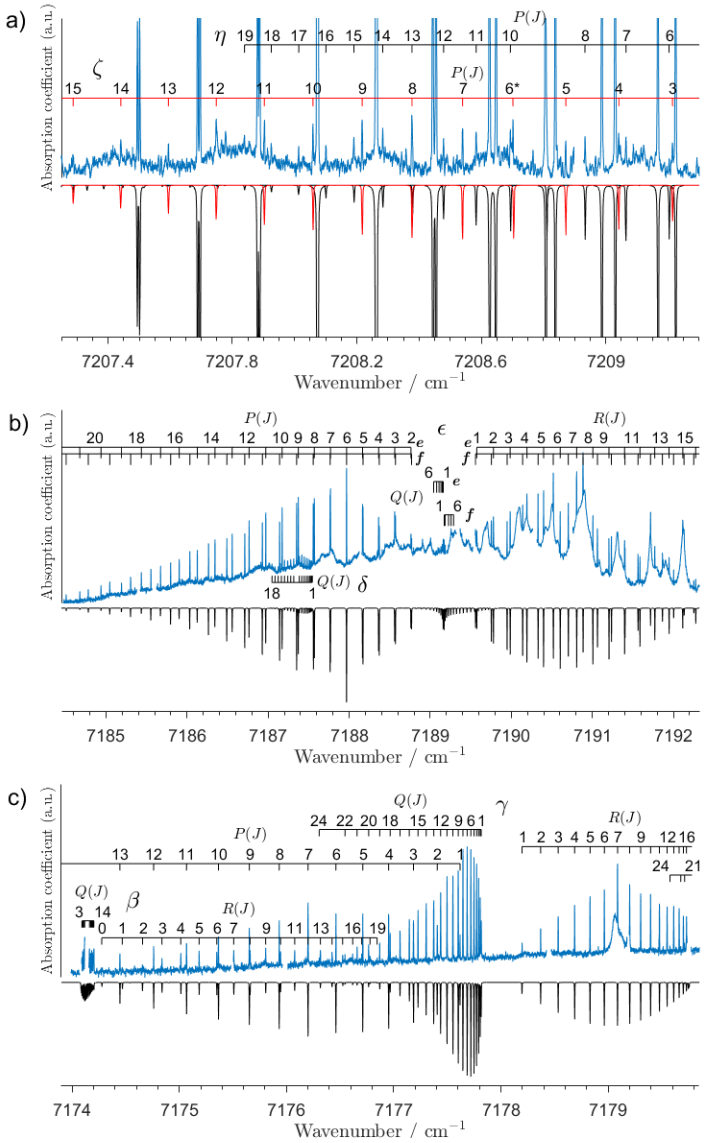

Figure 6. Portions of absorption spectrum of Ar-H_2O recorded in the 2OH stretch region using the improved FANTASIO set-up. In each panel, the experimental and simulated spectra are depicted in blue and black, respectively. The rotational temperature of the complex in the simulations was fixed at 13 K. Blank regions in the measured spectra are due to strong water monomer absorptions. Strong and broad absorption features in the baselines are assigned to the H_2O dimer [28,29]. ***Top panel**: Close up of the observed spectrum of the $\Sigma^e(0_{00}),(101) \leftarrow \Sigma^e(1_{01}),(000)$ of Ar-$H_2{}^{18}O$ with the simulated spectrum in red and $\Pi(1_{01}),(200) \leftarrow \Sigma^e(1_{01}),(000)$ sub-band of Ar-$H_2{}^{16}O$. The $\Pi(1_{10}),(200) \leftarrow \Pi(1_{01}),(000)$ sub-band of Ar-$H_2{}^{16}O$, denoted A in Ref.* [11], *is also shown and corresponds to the strong observed and simulated transitions. The transition labeled with an asterisk is perturbed.* ***Middle panel**: Spectrum of the $\Pi(1_{10}),(200) \leftarrow \Pi(1_{01}),(000)$ and the unassigned δ sub-bands of Ar-$H_2{}^{16}O$.* ***Bottom panel**: Spectrum of the $\Sigma^e(1_{01}),(200) \leftarrow \Pi(1_{10}),(000)$ and $\Pi(1_{01}),(200) \leftarrow \Sigma^f(1_{10}),(000)$ sub-bands of Ar-$H_2{}^{16}O$.*

Assignment of the ortho sub-bands

As can be seen in Table 2, three ortho sub-bands, β, ϵ, and η, are assigned to the same upper sub-state $\Pi(1_{01}),(200)$. The $\Pi(1_{01}),(200) \leftarrow \Pi(1_{10}),(000)$ sub-band around 7189 cm^{-1} is illustrated in Fig. 6b. The doublets in the *P*, *Q*, and *R*-branches are the signature of a $\Pi \leftarrow \Pi$ sub-band. The lower state combination differences and the intensity of the sub-band indicate that the lower sub-state is $\Pi(1_{10}),(000)$. The upper sub-state position near the 1_{01} rotational level of H_2O in (200) and the use of the predictions from Vanfleteren *et al.* [11] provide support for the assignment of the upper sub-state to $\Pi(1_{01}),(200)$.

The sub-bands β and η were assigned following the analysis of the ϵ sub-band and the known lower state constants from Ref. [11]. The higher frequency part of the $\Pi(1_{01}),(200) \leftarrow \Sigma^f(1_{10}),(000)$ (β) sub-band is illustrated in Fig. 6c. Note that the $\Pi(1_{01}),(200) \leftarrow \Sigma^e(1_{01}),(000)$ sub-band is ~~forbidden and~~ only weakly allowed, resulting from the anisotropy of the Ar-H_2O potential energy surface [30].

The $\Sigma^e(1_{01})$, $(200) \leftarrow \Pi(1_{10}),(000)$ (γ) is the strongest sub-bands observed in this work, lying close to the β sub-band. This band shows a clear *P*, *Q*, and *R*-branches, as presented in Fig. 6c. The absence of *R*(0) transition and the presence of *P*(1) and *Q*(1) transitions unequivocally indicate a $\Sigma \leftarrow \Pi$ sub-band. The relative position of this sub-band compared to the $\Pi(1_{01}),(200) \leftarrow \Pi(1_{10}),(000)$ sub-band (~ 11 cm^{-1} lower in frequency) and lower state combination differences provide support for the assignment of the γ sub-band as $\Sigma^e(1_{01}),(200) \leftarrow \Pi(1_{10}),(000)$. Indeed, the splitting between the $\Pi(1_{01}),(200)$ and $\Sigma(1_{01}),(200)$ sub-states was predicted to be 10.691 cm^{-1} [11], close to the observed value of 11.445 cm^{-1} (see Table 2).

The fitted upper sub-states constants from the assignment of the ortho sub-bands as discussed above are listed in Table 4. The lower states constants were fixed to the values obtained by Vanfleteren *et al.* [11]~~. in their global fit are also listed in this table.~~

Table 4. Molecular parameters for ortho Ar-$H_2{}^{16}O$ (in cm^{-1}) [a]

Sub-state	*e*/*f*	ν_0	*B*	B_{Calc} [b]	$D(\times10^6)$	$H(\times10^9)$	$L(\times10^{12})$
$\Sigma(1_{01})$, (000)[c,d]	*e*	0	0.10056170	0.1002	2.42083	0.0398	0.0479[g]
$\Pi(1_{10})$, (000)[c,d]	*e*	11.4291937	0.098465657	0.0981	4.4762[g]	-0.23068[g]	-0.087[g]
	f	11.4291937	0.098465657	0.0981	3.8359[g]	0.02818[g]	-0.042[g]
$\Sigma(1_{10})$, (000)[c]	*f*	36.1462535	0.09850834	0.0979	3.7374	-0.69	-0.355[g]
$\Sigma(1_{01})$, (200)	*e*	7198.88202(21)	0.0964680(41)	0.1001	2.094(18)	-0.554(20)	
$\Pi(1_{01})$, (200)	*e*	7210.32711(13)	0.1019278(31)	0.0979	5.944(17)	0.781(25)	
	f	7210.32711(13)	0.0985243(31)	0.0979	4.774(17)	0.409(25)	

[a] Quantities in parentheses are 1σ from the least-squares fit, in units of the last quoted digits.
[b] Value of *B* calculated in Ref. [11].
[c] Fixed ground state constants from Ref. [11].
[d] Sub-states coupled by a Coriolis interaction (see Ref. [11]), with a coupling constant (denoted as β in Ref. [11]) fixed at 0.1391903 cm^{-1}.
[g] Typos in Table VIII of Ref. [11] are corrected here for values that differed from their Pgopher simulations.

Discussion on the tentative assignments of the δ and θ sub-bands

For the δ sub-band, only a weak *Q*-branch is observed as illustrated in Fig. 6b. The first line of the branch seems to be *Q*(1) considering the intensity pattern at a rotational temperature of 13 K. Hence this sub-band should arise from a Σ or a Π sub-state of Ar-H_2O. None of the numerous possibilities using ground states and upper states constants from Ref. [11] and this work could reproduce the observed structure. One possibility is that this band arises from the double excitation of the intermolecular of the van der Waals stretch, i.e. $2\Sigma(0_{00})$ or $2\Sigma(1_{01})$ but the lack of spectroscopic information on these states prevents us from making a conclusive assignment.

The θ sub-band at 7223.5 cm^{-1} (not presented in figures) shows a strong *Q*-branch and possibly *P* and *R* transitions, however, it is strongly perturbed. The *Q*-branch itself seems to be perturbed. Furthermore, it is unclear if *Q*(1) is present. We are unable to assign this sub-band.

All the assigned transitions from the discussion above and the observed tentatively assigned transitions from sub-band δ can be found in the supplementary material. The root-mean-square deviation of the fit of the newly assigned sub-bands in the 2OH stretch region is equal to 0.00072 cm^{-1}.

Conclusions

A new pulsed slit valve (along with other improvements) was implemented in the FANTASIO spectrometer. The design of this slit was validated through Schlieren imaging, MW spectroscopy and near infrared continuous-wave CRDS.

The combination of information gathered with each technique allowed to ensure the collimation of the molecular beam, the production of large clusters by observation of the rotational lines of water heptamer and an improved sensitivity through the observation of the spectral signature of Ar-$H_2{}^{18}O$ observed in

natural abundance (0.2% of Ar-$H_2{}^{16}O$). In particular, the observation of $H_2{}^{18}O$-Ar, in natural abundance, in the overtone region represents a new standard in terms of sensitivity in high-resolution optical spectroscopy of van der Waals complexes.

~~The~~ This higher sensitivity of the spectrometer was then used to revisit the 2OH stretch region of Ar-H_2O complementing the study of Vanfleteren *et al.* [11]. The spectra were analyzed by considering a pseudo-diatomic model for the complex and a total of 7 new sub-bands were observed and analyzed. These sub-bands include a hot band involving the van der Waals stretch as the initial state. Our work complements the work of Vanfleteren *et. al.* [11] and ends the spectral characterization of this complex in the 2OH range. This contribution allows to provide a broad picture for theoreticians to properly model the spectral signature in the overtone of this very floppy and weakly bounded van der Waals complex. The benchmarking of theoretical calculations of spectral properties in the overtone range is supported by the recent publications of theoretical studies performed to decipher the spectral signature in the overtone region of for example the water dimer [29].

~~All these~~ Finally, the presented experimental improvements allow us to envision studies of Ar-water and possibly additional molecular complexes in even higher overtone ranges with the FANTASIO set-up, to hopefully address photo-induced reactivity. It also permits to consider the study of very large clusters using MW spectroscopy. This report represents a significant step in the evolution of the FANTASIO spectrometer.

Acknowledgements

The financial support of the FNRS through the « Mandat d'impulsion (MIS) » F.4038.24 and CDR J.0129.20 and J.0113.23 and of the Fédération Wallonie-Bruxelles through the Action de Recherches Concertées (ARC, grant number ARC iBEAM-18/23-090) is gratefully acknowledged. R.G. is a FRIA grantee of the Fonds de la Recherche Scientifique (FNRS) and thanks the financial support of UCLouvain and the Fédération Wallonie-Bruxelles through Fonds Spéciaux de Recherche (FSR) and ARC. N.M.-A. acknowledge the Natural Sciences and Engineering Research Council of Canada for its financial support. We warmly thank the service SQUARES of ULB for the loan of the FANTASIO setup.

References

[1] A. Amirav, U. Even, and J. Jortner, Chem. Phys. Lett. **83**, 1 (1981).
[2] C.M. Lovejoy and D.J. Nesbitt, Rev. Sci. Instrum. **58**, 807 (1987).
[3] K. Liu, R.S. Fellers, M.R. Viant, R.P. McLaughlin, M.G. Brown, and R.J. Saykally, Rev. Sci. Instrum. **67**, 410 (1996).
[4] M.A. Suhm and F. Kollipost, Phys. Chem. Chem. Phys. **15**, 10702 (2013).
[5] C. Abeysekera, B. Joalland, Y. Shi, A. Kamasah, J.M. Oldham, and A.G. Suits, Rev. Sci. Instrum. **85**, 116107 (2014).
[6] J. Langenhan, Ph.D. thesis, Humboldt-Universität zu Berlin, 2019.
[7] J.L. Neill, B.J. Harris, A.L. Steber, K.O. Douglass, D.F. Plusquellic, and B.H. Pate, Opt. Express **21**, 19743 (2013).
[8] M. Herman, K. Didriche, D. Hurtmans, B. Kizil, P. Macko, A. Rizopoulos, and P.V. Poucke, Mol. Phys. **105**, 815 (2007).
[9] K. Didriche, C. Lauzin, T. Földes, X. De Ghellinck D'Elseghem Vaernewijck, and M. Herman, Mol. Phys. **108**, 2155 (2010).
[10] M. Herman, T. Földes, K. Didriche, C. Lauzin, and T. Vanfleteren, Int. Rev. Phys. Chem. **35**, 243 (2016).
[11] T. Vanfleteren, T. Földes, M. Herman, J. Liévin, J. Loreau, and L.H. Coudert, J. Chem. Phys. **147**, 014302 (2017).
[12] T. Vanfleteren, T. Földes, and M. Herman, Chem. Phys. Lett. **627**, 36 (2015).
[13] K. Didriche and T. Földes, J. Chem. Phys. **138**, 104307 (2013).
[14] R.C. Cohen, K.L. Busarow, K.B. Laughlin, G.A. Blake, M. Havenith, Y.T. Lee, and R.J. Saykally, J. Chem. Phys. **89**, 4494 (1988).
[15] R.C. Cohen, K.L. Busarow, Y.T. Lee, and R.J. Saykally, J. Chem. Phys. **92**, 169 (1990).
[16] R.C. Cohen and R.J. Saykally, J. Chem. Phys. **95**, 7891 (1991).
[17] G.T. Fraser, F.J. Lovas, R.D. Suenram, and K. Matsumura, J. Mol. Spectrosc. **144**, 97 (1990).

[18] L. Zou and S.L. Widicus Weaver, J. Mol. Spectrosc. **324**, 12 (2016).
[19] R. Glorieux, A.J. Barclay, C. Lauzin, A.R.W. McKellar, and N. Moazzen-Ahmadi, Mol. Phys. e2259012 (2023).
[20] A.S. Bogomolov, A. Roucou, R. Bejjani, M. Herman, N. Moazzen-Ahmadi, and C. Lauzin, Chem. Phys. Lett. **774**, 138606 (2021).
[21] I.E. Gordon, L.S. Rothman, R.J. Hargreaves, R. Hashemi, E.V. Karlovets, F.M. Skinner, E.K. Conway, C. Hill, R.V. Kochanov, Y. Tan, P. Wcisło, A.A. Finenko, K. Nelson, P.F. Bernath, M. Birk, V. Boudon, A. Campargue, K.V. Chance, A. Coustenis, B.J. Drouin, J. –M. Flaud, R.R. Gamache, J.T. Hodges, D. Jacquemart, E.J. Mlawer, A.V. Nikitin, V.I. Perevalov, M. Rotger, J. Tennyson, G.C. Toon, H. Tran, V.G. Tyuterev, E.M. Adkins, A. Baker, A. Barbe, E. Canè, A.G. Császár, A. Dudaryonok, O. Egorov, A.J. Fleisher, H. Fleurbaey, A. Foltynowicz, T. Furtenbacher, J.J. Harrison, J.-M. Hartmann, V.-M. Horneman, X. Huang, T. Karman, J. Karns, S. Kassi, I. Kleiner, V. Kofman, F. Kwabia-Tchana, N.N. Lavrentieva, T.J. Lee, D.A. Long, A.A. Lukashevskaya, O.M. Lyulin, V.Yu. Makhnev, W. Matt, S.T. Massie, M. Melosso, S.N. Mikhailenko, D. Mondelain, H.S.P. Müller, O.V. Naumenko, A. Perrin, O.L. Polyansky, E. Raddaoui, P.L. Raston, Z.D. Reed, M. Rey, C. Richard, R. Tóbiás, I. Sadiek, D.W. Schwenke, E. Starikova, K. Sung, F. Tamassia, S.A. Tashkun, J. Vander Auwera, I.A. Vasilenko, A.A. Vigasin, G.L. Villanueva, B. Vispoel, G. Wagner, A. Yachmenev, and S.N. Yurchenko, J. Quant. Spectrosc. Radiat. Transf. **277**, 107949 (2022).
[22] A. Mazumdar, Columbia University Computer Science Technical Report, № CUCS-016-13, 2013.
[23] B.W. McCormick, in *Encyclopedia of Physical Science and Technology*, edited by R.A. Meyers, Third Edition (Academic Press, New York, 2003), pp. 621–630.
[24] G.G. Brown, B.C. Dian, K.O. Douglass, S.M. Geyer, S.T. Shipman, and B.H. Pate, Rev. Sci. Instrum. **79**, 053103 (2008).
[25] C. Pérez, M.T. Muckle, D.P. Zaleski, N.A. Seifert, B. Temelso, G.C. Shields, Z. Kisiel, and B.H. Pate, Science **336**, 897 (2012).
[26] E. Zwart, J.J. ter Meulen, W. Leo Meerts, and L.H. Coudert, J. Mol. Spectrosc. **147**, 27 (1991).
[27] C.M. Western, J. Quant. Spectrosc. Radiat. Transf. **186**, 221 (2017).
[28] N. Suas-David, T. Vanfleteren, T. Földes, S. Kassi, R. Georges, and M. Herman, J. Phys. Chem. A **119**, 10022 (2015).
[29] E. Vogt, I. Simkó, A.G. Császár, and H.G. Kjaergaard, J. Phys. Chem. A **127**, 9409 (2023).
[30] J.M. Hutson, J. Chem. Phys. **92**, 157 (1990).